The Astrophysical Journal, 719:1750–1758, 2010 August 20 doi:10.1088/0004-637X/719/2/1750

OBSERVATIONS OF CHROMOSPHERIC FLARE RE-BRIGHTENINGS

C. H. Miklenic[1,2], A. M. Veronig[2], B. Vršnak[3], and M. Bárta[4,5]
[1] Space Research Institute, Austrian Academy of Sciences, Schmiedlstraße 6, A-8042 Graz, Austria; christiane.miklenic@uni-graz.at
[2] Institute of Physics, University of Graz, Universitätsplatz 5, A-8010 Graz, Austria
[3] Hvar Observatory, Faculty of Geodesy, Kačićeva 26, HR-1000 Zagreb, Croatia
[4] Astronomical Institute of the Academy of Sciences of the Czech Republic, 25165 Ondřejov, Czech Republic
[5] Max Planck Institute for Solar System Research, D-37191 Katlenburg-Lindau, Germany
Received 2010 January 27; accepted 2010 June 28; published 2010 August 3

ABSTRACT

We investigate an active region that produced three C-class flares and one M-class flare within 2.5 hr. The morphology and location of the C-flares indicate that these events constitute a set of homologous flares. Radio observations indicate the occurrence of a downward-moving plasmoid during the impulsive phase of the M flare. We use *TRACE* 1700 Å filtergrams and *SOHO* Michelson Doppler Imager magnetograms to examine the character of the UV brightenings; i.e., we search for re-brightenings of former flare areas both across the series of events and within one and the same event. We find that essentially the same footpoints re-brighten in each C flare. Based on the progression of both the derived magnetic flux change rate and the observed Radio Solar Telescope Network microwave emission, we speculate about a further re-brightening during the decay phase of the M flare as a further member of the series of homologous flares. We conclude that the "postflare" field is driven to repeated eruption by continuous, shear-increasing, horizontal, photospheric flows, as one end of the involved magnetic arcade is anchored in the penumbra of a large sunspot. The observed motion pattern of the UV kernels indicates that the arcade evolves during the series of events from a both highly sheared and heavily entangled state to a still sheared but more organized state.

Key words: Sun: activity – Sun: chromosphere – Sun: corona – Sun: flares

Online-only material: animations, color figures

1. INTRODUCTION

In many active regions, solar flares tend to recur in periods of hours or days. If the members of such a series of flares share essentially the same footpoints and exhibit a nearly identical general shape when observed in Hα or extreme UV (EUV), they are called homologous flares (e.g., Waldmeier 1938; Woodgate et al. 1984). Even though homologous flares are a special type of flares, their study may improve our understanding of the flare phenomenon as a whole. Their location shows which particular sites in an active region are subject to instabilities leading to the release of flare energy (Martres 1989). The preflare conditions at these sites (e.g., high magnetic shear across polarity inversion lines near the footpoints, horizontal photospheric flows in the flare vicinity) may be particularly relevant for the initiation of a flare (Woodgate et al. 1984). Homologous flares also pose questions about the changes each member of the series initiates in the magnetic configuration of the active region. If the preflare conditions remain unchanged after the first flare, there must be some mechanism responsible for the end of the first and the onset of the subsequent event. In contrast, if the preflare conditions are destroyed by the first flare, they have to be rebuilt in order that the next flare can exhibit a similar morphology. New emerging flux at an opportune location (e.g., Ranns et al. 2000) and interactions between long-lived loops (Pohjolainen 2003) may be responsible for reforming the preflare conditions after each event. Simulations of continuous footpoint motions increasing the magnetic shear of a magnetic loop arcade have also been discussed as a means of rebuilding the preflare conditions (Choe & Cheng 2000). Another open question concerns the energy released in a series of homologous flares. We know that similar amounts of energy are released by each member of the series, but we do not know over which period the total energy released in the series is accumulated. Is the buildup of this energy a continuous process, interrupted by sudden energy release episodes, namely, the particular flare events, or does the set of homologous flares rather reflect the stepwise transition of a system, containing excess energy stored in the magnetic field, back to its lowest energy state, i.e., a potential field configuration?

In a series of homologous flares, the same area may brighten up in each member of the series. In principle, the occurrence of re-brightenings of former flare areas due to repeated energization of the same footpoints is also conceivable within one and the same event. Yet, such re-brightenings have never been observed before, and according to the standard model of two-ribbon flares, commonly referred to as CSHKP model (e.g., Carmichael 1964; Sturrock 1966; Hirayama 1974; Kopp & Pneuman 1976; Forbes & Priest 1984; Forbes & Lin 2000), they are indeed impossible, as energy is deposited at a particular location only once in the course of a flare, namely, at the frontal edges of the separating flare ribbons. However, the CSHKP model is a simplistic 2.5-dimensional view. The actual processes in the flaring region are probably much more complex. For instance, recent MHD simulations addressing the formation and evolution of plasmoids in the flare current sheet suggest that energy might be deposited at a particular location in the chromosphere more than once, namely, when a downward-moving plasmoid coalesces with the system of postflare loops by magnetic reconnection (Bárta et al. 2008). Accordingly, chromospheric re-brightenings within one and the same event cannot be ruled out. In contrast to the separating flare ribbons in the standard scenario, re-brightenings due to plasmoid/flare loop interactions are expected to appear at the footpoints of the system of postflare loops, i.e., behind the ribbons. In addition, re-brightened patches located in

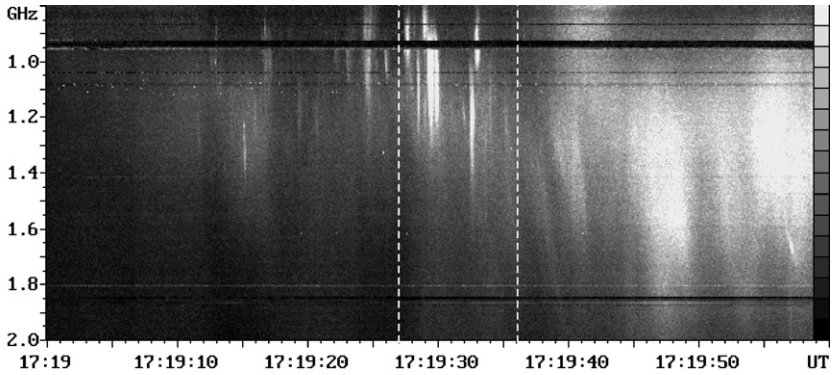

Figure 1. 0.8–2.0 GHz radio spectrum showing the drifting pulsating structure, observed by the Ondřejov radiospectrograph between 17:19:14 UT and 17:19:35 UT on 2004 July 23, i.e., in the impulsive phase of the M flare. Initially, the DPS exhibits a negative frequency drift, changing to a positive drift after 17:19:27 UT. The vertical lines mark the period of positive frequency drift, corresponding to the downward motion of the plasmoid.

opposite magnetic polarity domains are predicted to approach each other, as during the plasmoid/loop interaction outer flare loops are affected before inner ones.

In this paper, we investigate an active region that produced three C-class flares and one M-class flare within 2.5 hr. The morphology and location of the C flares indicate that these events constitute a set of homologous flares. Radio observations indicate the existence of a downward-moving plasmoid during the impulsive phase of the M flare. We examine the character of the flare brightenings; i.e., we concentrate on the detection of chromospheric re-brightenings of former flare areas both across the series of events and within one and the same event. The paper is organized as follows. In Section 2, we describe the data sets that were used and observations. The analysis is presented in Section 3. In Section 4, we summarize our results. Discussion and conclusions are given in Sections 5 and 6, respectively.

2. DATA AND OBSERVATIONS

On 2004 July 23, NOAA Active Region 10652 produced three *GOES* class-C flares and one M flare near the center of the solar disk (N07° W04°) within 2.5 hr. The first flare (C1.1, onset approx. 16:04 UT) was associated with a fast halo-CME (first LASCO C2 appearance 16:06 UT, linear velocity ∼820 km s^{-1}; CME details are obtained from the *Solar and Heliospheric Observatory* (*SOHO*) LASCO CME catalog[6]; Yashiro et al. 2004). Another CME was launched from AR 10652 (first LASCO C2 appearance 17:54 UT, linear velocity ∼570 km s^{-1}) in association with either the second or the third flare (C1.7 and M2.2, with onset times of approx. 17:10 UT and 17:18 UT, respectively). The last flare in the series of events under study is a C4.2 flare, starting at approx. 18:04 UT. The morphology and location of the C flares indicate that they constitute a set of homologous flares, occurring approx. one hour apart.

Radio observations provided by the Ondřejov radiospectrograph (Jiřička et al. 1993) show the occurrence of a drifting pulsating structure during the impulsive phase of the M flare. Drifting pulsating structures (DPS) are numerous, fast-drifting type III-like or even U-type features with a particularly low global frequency drift. They are interpreted as the radio signatures of plasmoids, formed in a disrupting current sheet (e.g., Kliem et al. 2000; Khan et al. 2002; Karlický 2004). The individual radio pulses are assumed to be generated by electrons that are trapped inside the plasmoid and accelerated during its formation, whereas the global frequency drift of the DPS reflects the motion of the plasmoid in the stratified solar atmosphere, with negative/positive frequency drift indicating upward/downward motion of the plasmoid. The DPS in the M flare (see Figure 1) appears at approximately 17:19:14 UT. Initially, it exhibits a negative frequency drift for 13 s, indicating upward motion of the plasmoid. After 17:19:27 UT the plasmoid reverses direction, indicated by a positive frequency drift of the DPS from approximately 800 MHz to 1400 MHz during a period of 7 s (frequency drift: 50 MHz s^{-1}, instantaneous frequency bandwith: 300 MHz).

We use the following data sets to examine the characteristics of the chromospheric brightenings in the four events under study.

1. An image time series in the 1700 Å passband, provided by the *Transition Region and Coronal Explorer* (*TRACE*; Handy et al. 1999). During the M2.2 flare the cadence was approx. 5 s, during the C flares it varied between roughly 43 and 90 s. Hα full-disk observations provided by the Big Bear Solar Observatory (BBSO; Denker et al. 1999) are also available. Because of saturation effects, we do not use the Hα images in the analysis but present an Hα movie of the flare evolution in the online material (see movie 1, associated with Figure 2).
2. Three successive full-disk line-of-sight magnetograms acquired one-minute apart by the Solar Oscillations Investigation/Michelson Doppler Interferometer (SOI/MDI) instrument (Scherrer et al. 1995) on board *SOHO*. These images were averaged together to form a single low-noise magnetogram, which was used in further analysis.
3. Microwave flux data with 1 s time resolution, obtained from the US Air Force Radio Solar Telescope Network (RSTN; Guidice et al. 1981). Flare-associated microwave gyrosynchrotron emission is produced by gyrating high-energy electrons. Flare-accelerated electrons carry a large fraction of the total energy released during a flare (e.g., Hudson 1991; Dennis et al. 2003). Therefore, we use the evolution of the microwave emission in the 8.8 GHz and 15.4 GHz RSTN channels as proxy for the evolution of the flare-energy release rate.

TRACE images were differentially rotated to the same reference time. Coalignment of *TRACE* and MDI data sets was accomplished using MDI continuum and *TRACE* WL images, accounting for the different pointings of the *TRACE* 1700 Å and WL telescopes. MDI images were converted from *SOHO*-view to Earth-view.

Figure 2 shows the flaring region (AR 10652, northern hemisphere) as well as a second active region in the southern

[6] http://cdaw.gsfc.nasa.gov/CME_list/

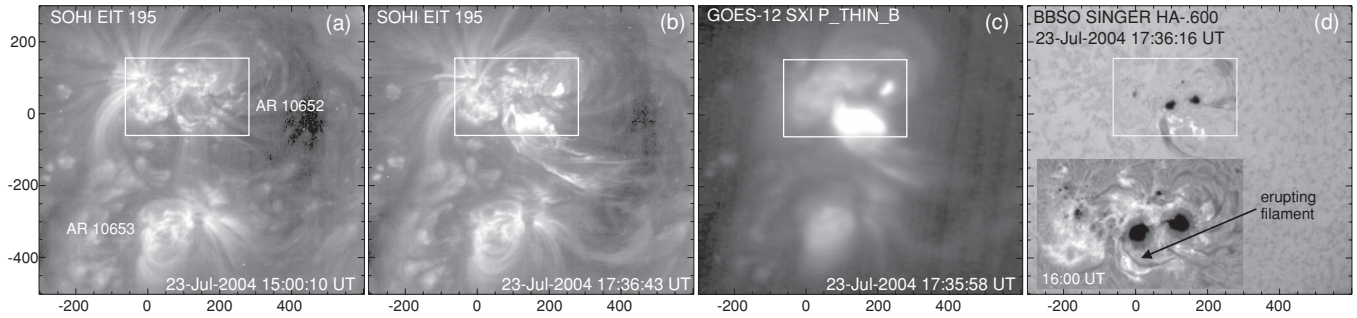

Figure 2. (a) Still from movie 2: *SOHO* EIT 195 Å preflare image of AR 10652 (northern hemisphere) and AR 10653 (southern hemisphere) connected by transequatorial interconnecting loops; (b) *SOHO* EIT 195 Å image taken during the decay phase of the M2.2 flare. Bright ejecta from an erupting filament in AR 10652 push aside a large loop system in the southern hemisphere (lower right corner); (c) still from movie 3: the ejecta are also visible in soft X-rays (GOES-12 SXI); (d) BBSO Hα image showing the M2.2 flare ribbons south of the two big sunspots as well as the ejecta. The inset is a still from movie 1 and shows an Hα preflare image of the flaring region, arrow pointing at the location of the erupting filament. The four white rectangles in panels (a)–(d) mark the region shown in the inset—field of view (FOV): $900'' \times 800''$.

(Animations of this figure are available in the online journal.)

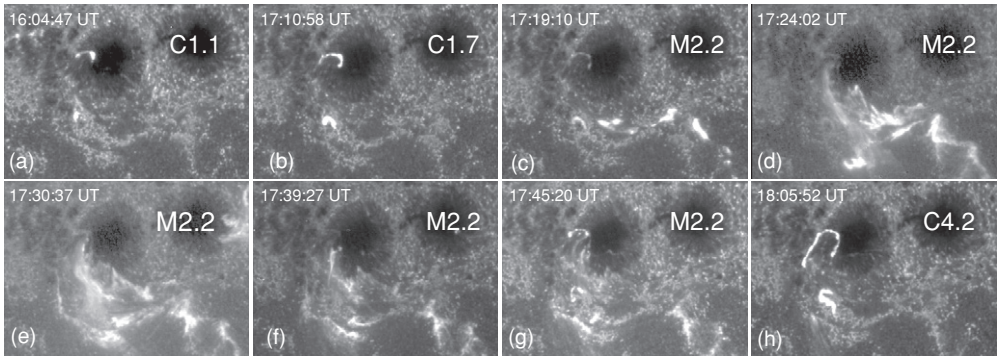

Figure 3. Flare evolution in *TRACE* 1700 Å. The *GOES* class of each of the four flares is shown in the upper right corner of each panel. Two small regions brighten up at the onset of the C1.1 flare (panel (a)); one in the penumbra of the eastern sunspot, the other one south of it. These regions re-brighten during the C1.7, M2.2, and C4.2 flares (panels (b), (g), and (h))—FOV: $194'' \times 160''$.

hemisphere (AR 10653). Both regions are connected before the onset of the first event of the series under study by transequatorial interconnecting loops (see Figure 2(a)). During the decay phase of the M2.2 flare, i.e., after approx. 17:28 UT, plasma is ejected from the flaring region, observed in emission (EUV and soft X-rays) and absorption (filament eruption in Hα). The ejecta hit a large loop system in the southern hemisphere and push it aside (see Figure 2, panels (b) and (c), and movies 2 and 3 of the online material).

Figure 3 shows an image sequence of the flaring region spanning the time range of the C1.1, C1.7, M2.2, and C4.2 flares under study. At the onset of the C1.1 event, two small regions brighten up; one in the penumbra of the eastern sunspot, the other one south of it. These regions re-brighten during the C1.7, M2.2, and C4.2 flares. Movies 1 (Figure 2) and 4 (Figure 4) of the online material show the evolution of all four events in BBSO Hα and *TRACE* 1700 Å, respectively.

3. ANALYSIS

Forbes & Priest (1984) and Forbes & Lin (2000) derived a quantitative estimate for the coronal reconnection rate or magnetic flux change rate $\dot{\varphi}$, respectively, that can be derived from observable photospheric and chromospheric quantities:

$$\dot{\varphi} = \frac{\partial}{\partial t} \int B_n \, da, \qquad (1)$$

where B_n is the photospheric magnetic field-strength component perpendicular to the solar surface inside the newly brightened flare area da. We use Equation (1) to determine both the magnetic flux change rate $\dot{\varphi}$ and the re-brightening rate $\dot{\varphi}_{\rm RB}$. The only difference is that calculating $\dot{\varphi}$ requires the measurement of B_n inside areas that brighten up for the first time, whereas in $\dot{\varphi}_{\rm RB}$ only those areas are included that brighten up more than once. Accordingly, peaks in the re-brightening rate signify that the same footpoints are energized repeatedly. In addition, such peaks allow an estimate of the corresponding magnetic flux.

The method to determine the magnetic flux change rate $\dot{\varphi}$ is described in detail in Miklenic et al. (2007, 2009) and only briefly outlined in the following. We use intensity thresholds in *TRACE* 1700 Å base difference images to correctly differentiate between flare pixels and non-flare pixels. We measure at each time t both the newly brightened area da in a *TRACE* image compared with the preceding images and the co-aligned MDI magnetic field strength B_n inside this area. We correct the reported MDI line-of-sight magnetic field values B as follows: $B_n = (1.56\,B)/\cos\theta$, where 1.56 is a correction factor, used to account for MDI saturation effects (Berger & Lites 2003), and θ is the central meridional distance of the flare. The $\cos\theta$-correction, used to derive a radial field at each pixel, is small, since the flaring region is close to disk center. We take the da and B_n measurements separately for each magnetic polarity domain, then we apply Equation (1) for both domains. This yields $\dot{\varphi}_+$ and $\dot{\varphi}_-$, i.e., the magnetic flux change rate for the positive and negative polarity domain. Finally, we calculate the magnetic flux change rate $\dot{\varphi}$ by taking the mean of $\dot{\varphi}_+$ and $\dot{\varphi}_-$. To determine the re-brightening rate $\dot{\varphi}_{\rm RB}$, we apply Equation (1) again for both domains and take the mean, but this time we

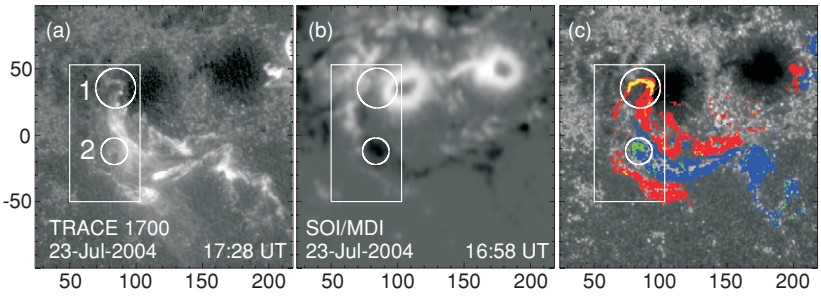

Figure 4. (a) Still from movie 4: *TRACE* 1700 Å filtergram of the flaring region at the time of the *GOES* maximum of the M2.2 flare; (b) MDI magnetogram (white: positive, black: negative polarity). The umbrae of the two sunspots are saturated. Data range scaled to [−1720, +3860] G out of [−2755, +4320] G; (c) still from movie 5: flare area superimposed on a *TRACE* 1700 Å preflare image. Red/yellow: newly brightened/re-brightened area in the positive polarity; blue/green: newly brightened/re-brightened area in the negative polarity—FOV: 194″ × 198″. Circles 1 and 2 mark the positions of the most prominent re-brightenings. The white rectangles show the FOV of Figures 6, 7, and 8.

(Animations and a color version of this figure are available in the online journal.)

consider only flaring areas *da* that re-brighten, i.e., brighten up more than once.

As mentioned before, we use intensity thresholds to determine whether a particular pixel at a particular time is a flaring or non-flaring pixel, i.e., is in its ON- or OFF-state. Usually, flare pixels show ON-OFF-sequences, corresponding to energy deposition at the footpoints of the newly reconnected field lines, associated plasma heating, and subsequent cooling. Saba et al. (2006) reported average ON-times for *TRACE* 1600 Å pixels of about 1 minute but also found ON-times spanning 3–4 minutes. After this, pixels switch to their OFF-state and remain there, provided that no further energy is deposited at the corresponding region in the chromosphere. However, if a pixel is energized more than once, it exhibits an ON-OFF-ON-sequence. Therefore, we search for such sequences at each pixel location to identify re-brightened areas. We define a re-brightened pixel as a pixel that: (1) was once newly brightened and is bright (ON) for some time; (2) is dark (OFF) for at least 10 minutes; and (3) exceeds the intensity threshold again (ON).

4. RESULTS

Figure 4 shows the flaring region in *TRACE* 1700 Å filtergrams at the time of the M2.2 *GOES* maximum (panel (a)), the coaligned MDI magnetogram (panel (b)), and the total flare area calculated from all four events superimposed on a *TRACE* 1700 Å preflare image (panel (c)). Red/blue patches highlight the newly brightened area in the positive/negative magnetic polarity domain, whereas yellow/green patches show the location of areas that re-brighten in the course of the flares. The two most prominent re-brightening zones are encircled in all three panels of Figure 4, with circle 1 lying in the positive and circle 2 in the negative polarity domain. There are also smaller areas where re-brightened pixels are found, but we focus on the areas inside circles 1 and 2, since these re-brightenings are most distinct.

In the left panel of movie 5 of the online material (see Figure 4), we present the temporal evolution of the detected newly and re-brightened areas superimposed on the *TRACE* 1700 Å images. The right panel of movie 5 shows the corresponding base difference images (a preflare image taken before the first event of the series was subtracted from all subsequent images). The color-codes and circles in the movie are the same as in Figure 4.

Figure 5 shows the *GOES* 1–8 Å soft X-ray (SXR) flux, covering all four flares under study (panel (a)), the 8.8 GHz RSTN radio flux (panel (b)), and the magnetic flux change rate $\dot{\varphi}$ along with the re-brightening rate $\dot{\varphi}_{RB}$ (panel (c)). The gray

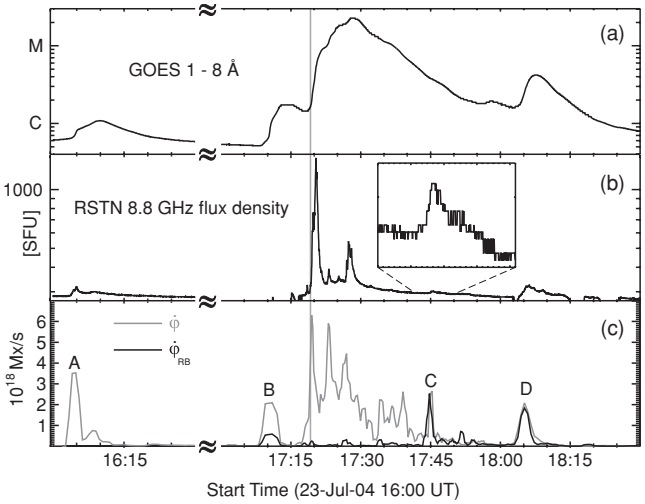

Figure 5. (a) *GOES*12 1–8 Å soft X-ray (SXR) profile; (b) RSTN flux density in solar flux units (SFU). Most of the features observed at 8.8 GHz are also present at 15.4 GHz, but with smaller amplitude. The inset shows a zoom of the radio flux from 17:42 to 17:50 UT, indicated by the dashed lines, with a peak-value of 302 SFU at 17:45 UT; (c) magnetic flux change rate $\dot{\varphi}$ (gray) and re-brightening rate $\dot{\varphi}_{RB}$ (black). The letters mark time intervals. The gray vertical line at approx. 17:19 UT highlights the observation time of the DPS. None of the profiles shows anything remarkable between 16:30 UT and 17:00 UT, so this time interval is excluded to save space.

vertical line in Figure 5 highlights the DPS observation time and the letters in Figure 5(c) mark time intervals, extending over the following periods: 16:04–16:10 UT (A), 17:09–17:11 UT (B), 17:44–17:45 UT (C), and 18:04–18:07 UT (D). The three most prominent peaks in the magnetic flux change rate $\dot{\varphi}$ occur during the impulsive phase of the M2.2 flare and in correlation with the highest peaks in the microwave gyrosynchrotron emission of flare-accelerated electrons, as expected from the standard model. During the decay phase of the M2.2 flare, $\dot{\varphi}$ exhibits several peaks, including the one around interval C. Except for a tiny bump around interval C (enlarged in the inset of Figure 5(b)), the radio flux remains quiet in this phase of the event, but the SXR flux shows some small bumps rather than a smooth gradual decay. The $\dot{\varphi}$-peaks around intervals A, B, and D are correlated with the onset of the C1.1, C1.7, and C4.2 flares. The radio flux contains bad data during interval B, but during A and D the peaks in the magnetic flux change rate are correlated with the peaks in the microwave emission. The re-brightening rate $\dot{\varphi}_{RB}$ exhibits three distinct peaks during time intervals B, C, and D, all of them synchronized with peaks in the magnetic flux change rate. Peaks in $\dot{\varphi}$ are higher than peaks in $\dot{\varphi}_{RB}$, if

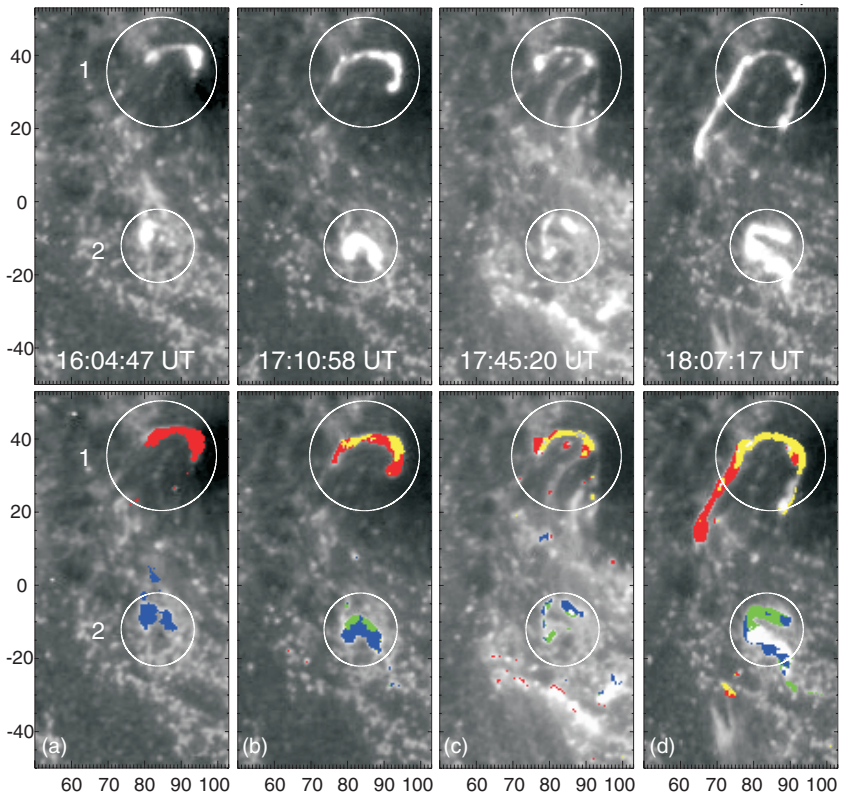

Figure 6. Top row: *TRACE* 1700 Å filtergrams taken at a particular time within intervals A, B, C, and D (corresponding to panels (a), (b), (c), and (d), respectively; see Figure 5(c)). Bottom row: areas that brighten up during the four time intervals are highlighted in color in the same images. Red/blue: newly brightened area in positive/negative magnetic polarity domain, yellow/green: re-brightened area in positive/negative domain—FOV: 53″ × 103″ (see white rectangles in Figure 4). Circles 1 and 2 are the same as in Figure 4.

(A color version of this figure is available in the online journal.)

both newly and re-brightened areas are located in regions with comparable magnetic field strength (interval B). On the other hand, if the usually smaller re-brightened areas are located in regions with higher magnetic field strength (intervals C and D), the amplitudes in both rates are comparable, since the stronger magnetic fields compensate the smaller size of the re-brightened areas.

Figure 6 presents closeups of the region marked by the white rectangles in Figure 4. The top row of Figure 6 shows snapshots taken at a particular time within each of the four intervals A–D. The same images are displayed in the bottom row of Figure 6, with areas that brighten up during these intervals highlighted in color. During interval A, areas located within the two circles brighten up for the first time (red/blue patches). During intervals B, C, and D, parts of the encircled areas re-brighten, indicated by the yellow and green patches. There are also new brightenings (red/blue) occurring within these time intervals.

The images in Figure 7 are snapshots taken at a particular time *between* the four time intervals to demonstrate the intermittent intensity decrease or even disappearance of the structures within circles 1 and 2. Between intervals A and B (left panel) all formerly brightened regions get dark again. Before interval C (middle panel), the structures that brightened up within circles 1 and 2 during interval B are barely discernible. After interval C (right panel), most parts of the bright structures within the two circles are relatively faint again, but there is still a bright patch in circle 2 that remains bright even beyond interval D (cf. white patch in bottom row of Figure 6, panel (d)).

Figure 8 shows the evolution of the newly brightened area (interval A) and re-brightened area (intervals B, C, and D).

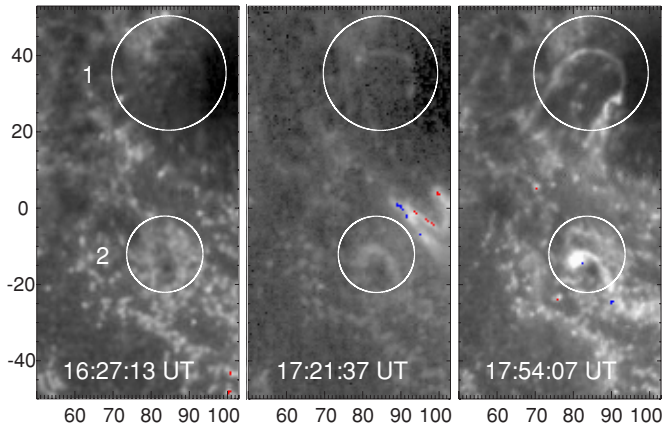

Figure 7. Snapshots taken at a particular time *between* intervals A, B, C, and D. Left: all newly brightened regions from interval A are dark again. Middle: the structures that brightened up within circles 1 and 2 during interval B (cf. bottom row of Figure 6, panel (b)) are barely discernible. Some newly brightened pixels (red, blue) appear top right of circle 2. Right: most parts of the bright structures within the two circles are relatively faint again, but there is still a bright patch in circle 2 that remains bright even beyond interval D—FOV: 53″ × 103″ (cf. white rectangles in Figure 4). Circles 1 and 2 are the same as in Figure 4.

(A color version of this figure is available in the online journal.)

Patches that brighten up at a particular time within each interval are color-coded. At the beginning of interval A, three bright flare kernels appear (blue patches in Figure 8, panel (a)). Near the end of the interval, a fourth kernel is formed (orange/red), but no distinct kernel motion is visible. During intervals B, C, and D (Figure 8, panels (b), (c), and (d)), the re-brightened

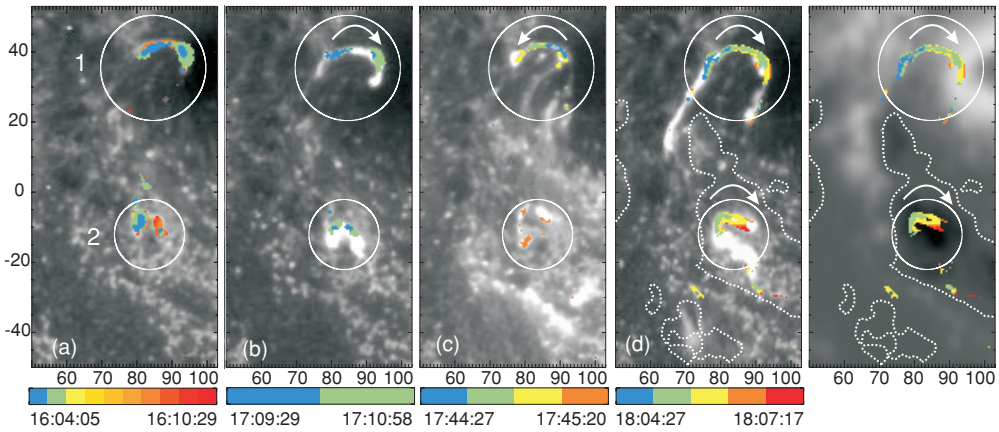

Figure 8. Evolution and apparent motion of the newly brightened area (time interval A; panel (a)) and re-brightened area (time intervals B, C, and D; panels (b), (c), and (d), respectively). Patches that brighten up at a particular time within each interval are superimposed in color-code on the top-row images shown in Figure 6, except for the rightmost panel, where the re-brightenings of interval D are superimposed on the MDI magnetogram. Begin and end of each time interval are given below the color bars. White arrows indicate the direction of the apparent kernel motion. Dotted lines: magnetic neutral line—FOV: 53″ × 103″ (cf. white rectangles in Figure 4). Circles 1 and 2 are the same as in Figure 4.

(A color version of this figure is available in the online journal.)

area in circle 1 exhibits an apparent motion. The direction of motion is reversed in each subsequent re-brightening (indicated by arrows in Figure 8). In circle 2, the re-brightened area shows a distinct motion only during interval D, but the re-brightenings in circles 1 (positive polarity) and 2 (negative polarity) do not approach each other. Instead, they exhibit a parallel motion. In the rightmost panel of Figure 8, the re-brightenings of panel (d) are superimposed on the MDI magnetogram. The dotted line is the polarity inversion line, which is rather intricate within this part of the flaring region.

5. DISCUSSION

In the following we briefly summarize the main results of the analysis and discuss their implications. The magnetic flux change rate $\dot{\varphi}$ and the microwave emission, which acts as a proxy for the evolution of the flare-energy release rate, are temporally correlated, as expected from the standard flare model. The most prominent peaks in the microwave flux occur during the impulsive phase of the M2.2 flare and are clearly reflected by the highest peaks in the magnetic flux change rate. The less pronounced microwave peaks during intervals A (C1.1 flare), C, and D (C4.2 flare) also appear in $\dot{\varphi}$.

We find two regions, located in opposite magnetic polarity domains, where distinct re-brightenings occur (see circles 1 and 2 in Figure 4(c)). The corresponding peaks in the re-brightening rate are synchronized with the peaks in the magnetic flux change rate. Does one of these repeated energizations of particular flare areas reflect plasmoid/flare loop interaction? The first re-brightening (interval B) can be discarded, as it appears *before* the DPS, observed in radio during the impulsive phase of the M flare (see Figure 5(c)). The subsequent re-brightenings (intervals C and D) occur a long time after the observation of the DPS (nearly 30 minutes and 45 minutes, respectively). However, if a chromospheric re-brightening is due to plasmoid/flare loop interactions, the corresponding peak in the re-brightening rate is expected to appear shortly after the observation of a downward-moving plasmoid. In addition, both the first and the ensuing energizations of the respective area must occur in one and the same flare. This is not the case here, since the first energization of areas inside circles 1 and 2 takes place in an earlier event, more than an hour before the DPS appears. Finally, the re-brightened patches, located in opposite magnetic polarity domains, do not approach each other. Therefore, we conclude that none of the detected re-brightenings can be interpreted as the chromospheric signature of the interaction of a downward-moving plasmoid with the system of postflare loops. Nevertheless, the existence of such re-brightenings cannot be ruled out, since our analysis is the first case study in this context. Further detailed analyses of flares associated with downward-moving plasmoids are necessary.

Do the detected re-brightenings constitute a set of homologous flares? Since in a series of such events essentially the same footpoints are re-brightening, the overall shape of each member of the series must be similar. Accordingly, we compare the morphology of the areas that brighten up during intervals A, B, C, and D (see the bottom row of Figure 6) and find that in each time interval these areas look similar. In addition, to some extent, exactly the same footpoints are energized in each repeated flaring. Therefore, we conclude that the three C flares (intervals A, B, and D) in fact constitute a set of homologous flares, approximately one hour apart. According to Martres (1989), this is a characteristic time lag between members of so-called "rafales" of homologous flares (rafales is the French word for a burst of machine-gun fire). The author lists some characteristic properties of such events. Bursts of homologous flares typically appear in series of three to five events close to sunspots, namely, at the edge of the penumbra of a large sunspot. Actually, Martres (1989) considers the presence of a large sunspot as a necessary condition for a burst of homologous flares. The location of the flare site in our observations, in particular the location of circle 1, fits in this view. Parts of the northern ribbon of the three C flares appear directly in the penumbra of a large sunspot, and other parts are at the edge of the penumbra.

Does the remaining re-brightening, the one during interval C, fit in our interpretation of a burst of homologous flares? During the M2.2 flare, the flaring region is large and the shape of the flare ribbons south of the sunspots is rather complex. However, the morphology of the re-brightenings detected during interval C in the decay phase of the M-flare is similar to the shape of the flare areas found in the three C flares. Therefore, we speculate that another homologous flare occurred at the location of circles

1 and 2 during interval C, but it did not appear in the *GOES* flux as a separate event, because it was masked in the decay phase of the M flare. We refer to the unusual progression of the *GOES* flux during the decay phase of the M flare. The *GOES* flux does not decrease smoothly but rather exhibits some small bumps, one of them occurring around interval C (cf. Figure 5(a)). This indicates temporary heating of the plasma filling the flare loops, while plasma cooling is already underway. In addition, the microwave flux density also shows a tiny bump around interval C (cf. inset of Figure 5(b)), indicating the acceleration of particles to nonthermal energies at this time. Therefore, we interpret the re-brightenings during interval C as a further member of the set of homologous flares. Furthermore, since homologous flares have similar energy (e.g., Benz 2000), we assume that the event was a *GOES* class C flare as well. The height of the bump in the observed *GOES* flux also suggests *GOES* class C for this event.

What caused the repeated flaring or the repeated energization of areas within circles 1 and 2, respectively? Movie 3 of the online material (see Figure 2) shows the repeated brightening of a roughly north–south-aligned soft X-ray loop arcade in the region of circles 1 and 2 (i.e., around $x = 90''$, $y = 10''$ from the center of the solar disk). These brightenings occur around 15:07 UT (i.e., before the time interval under study) and during the C1.1 and C1.7 flares (∼16:06 UT and 17:12 UT). During interval C and also during the C4.2 flare (∼17:44 UT and 18:06 UT, respectively), the SXR loop arcade is indistinguishable from the vast soft X-ray brightenings associated with the M2.2 flare, due to saturation effects. Nevertheless, the times of appearance of the arcade as well as its location and orientation indicate that the arcade connects areas in circles 1 and 2. Therefore, it appears that the set of homologous flares occurs at the site of a magnetic arcade that is repeatedly driven to erupt and relaxes back to its "initial" topology after each event. What mechanism is at the bottom of this field evolution?

Choe & Cheng (2000) presented a numerical MHD model, which provides an explanation of the recurrence of homologous flares. The authors investigated the evolution of magnetic arcades in a resistive plasma subject to shear-increasing footpoint motions (i.e., motions parallel to the magnetic neutral line and converging footpoint motions). Initially, magnetic reconnection of the field lines of the line-tied arcade creates a magnetic island. The reconnection also divides and redistributes the toroidal flux previously contained in line-tied flux tubes into two new flux systems: the magnetic island and the underlying arcade with its still line-tied footpoints. After island formation, the magnetic shear in the arcade is reduced, but it increases again due to a continuing shearing motion. As soon as a critical shearing value is reached, reconnection sets in again to form a second magnetic island. This newborn island rises and pushes up the line-tied field lines surrounding it. As a consequence, these field lines reconnect with the field lines of the initially created upper island. After all line-tied field lines in the arcade surrounding the newborn island have reconnected with the upper island, the newborn island is no longer obstructed, and thus, can rise quickly. As both magnetic islands carry currents flowing in the same direction, they approach each other, merge by magnetic reconnection of their field lines, and form an integrated island. The field lines surrounding this island continue to reconnect in the vertical current sheet below. As a result, the integrated island is supplied with new poloidal flux, and thus, its upward motion is facilitated. Choe & Cheng (2000) consider the sequence of (1) generation of a newborn island by magnetic reconnection, (2) merging of upper and newborn island, and (3) reconnection below the integrated island as an individual flare, and interpret the repetitive occurrence of this sequence as a set of homologous flares.

Is it likely that the magnetic arcade connecting circles 1 and 2 was subject to continuous, shear-increasing footpoint motions, and thus, driven to repeated eruption? First of all, we note that the region around circles 1 and 2 is magnetically complex. Circle 2 is located in a tongue-shaped region of negative magnetic polarity, embedded in an area of positive magnetic fields. Thus, the polarity inversion line (PIL) is intricate (see the rightmost panel of Figure 8): the relevant part of the PIL is bent to two roughly north–south-aligned sections between circles 1 and 2. Together with the north–south alignment of the connecting soft X-ray loops, this indicates a highly sheared magnetic field configuration in the flaring region. In addition, we emphasize that the northern ribbon of the series of homologous flares is anchored in the penumbral region of a large sunspot (see circle 1 in Figure 4(c)). The edge of a sunspot is a very dynamic region, in which continuous, horizontal flows are directed away from the sunspot. Therefore, at least the northern end of the arcade was probably subject to continuous, horizontal, photospheric flows that might have provided the sustained shearing, required to repeatedly trigger magnetic reconnection in the arcade. As a consequence, a series of newborn magnetic islands may have been created.

The evolution and apparent motion of the UV kernels is a further interesting detail in this series of homologous flares. We find that the re-brightened patches in circle 1 move along the northern flare ribbon during intervals B, C, and D. The direction of motion is reversed in each subsequent re-brightening (see Figure 8). In contrast, the kernels in circle 2 show no distinct motion during the first three time intervals. Only during interval D, we detect a systematic kernel motion in the southern ribbon, parallel to the kernel motion in the northern ribbon. In simple reconnection models, for instance, in the CSHKP model, kernel motions perpendicular to both the flare ribbons and the polarity inversion line are expected. However, there are numerous observations in hard X-rays and also in Hα showing footpoint motions parallel and antiparallel to the polarity inversion line (e.g., Fletcher & Hudson 2002; Bogachev et al. 2005; Grigis & Benz 2005; Temmer et al. 2007; Gan et al. 2008; Lee & Gary 2008). Wang (2009) reported a prevalence of UV kernel motions along the iso-Gauss contours over those along the gradient of the magnetic field. Krucker et al. (2003) investigated the hard X-ray (HXR) source motion of a γ-ray flare and found a motion pattern quite similar to our findings during intervals B and C. The authors reported that one of the HXR footpoints moved along one of the flare ribbons, indicating high shearing of the reconnected magnetic field lines, while the two sources on the other ribbon did not move systematically. Krucker et al. (2003) concluded that the observed motion pattern reflects a complicated configuration of the sheared magnetic arcade. Although the authors studied HXR source motions, they reported that each of the sources had counterparts in EUV and Hα, with the Hα kernels showing a similar motion as the HXR footpoints. Therefore, we apply the explanation by Krucker et al. (2003) to our findings.

We suggest that the series of homologous C flares occurred in a highly sheared loop arcade, which was additionally characterized by a complicated magnetic configuration. Figure 9 illustrates the proposed evolution of the magnetic configuration during the series of events, inferred from the motion pattern of the UV kernels. During the first C flare (interval A), the

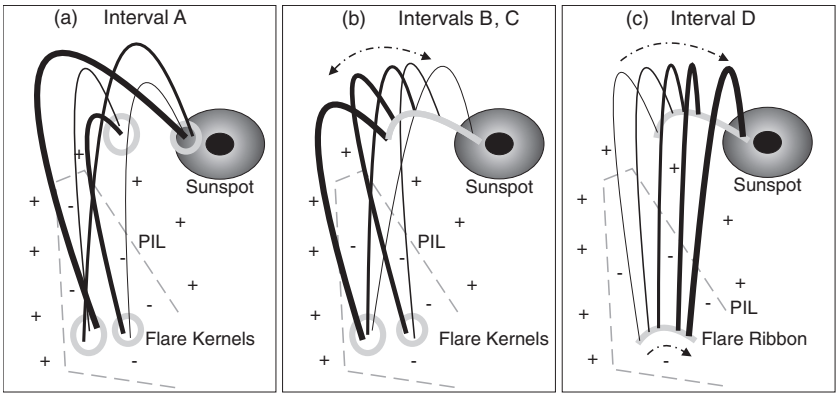

Figure 9. Magnetic field configuration inferred from the motion pattern of the UV kernels during the set of homologous flares. Panels (a)–(c) illustrate the effect of the reconnection processes in each flare. The magnetic arcade evolves from a highly sheared and heavily entangled state to a still sheared but more organized state. The curved black lines depict the loops of the magnetic arcade. The increasing thickness of the loops represents the successive times of brightening of the corresponding footpoints. Dashed-dotted arrows indicate the direction of a systematic kernel motion. The + and − symbols represent areas of positive and negative magnetic polarity. The dashed gray line is the PIL. The light-gray solid circles and curved lines mark UV flare kernels and ribbons.

loops are heavily entangled. As a consequence, newly reconnected field lines and previously reconnected field lines are not rooted adjacent to each other but have disorganized footpoints (i.e., footpoints at scattered locations) in both magnetic polarities (see Figure 9(a)). Therefore, no systematic kernel motion is observed. The reconnection process during this flare, however, changes the magnetic connectivity of the footpoints in such a way that during intervals B and C consecutively reconnected field lines have regularly ordered footpoints in the positive polarity, while the corresponding footpoints in the negative polarity are still disorganized (see Figure 9(b)). As a result, we observe a systematic kernel motion, creating a flare ribbon, only in one magnetic polarity domain, while the unsystematic jumps of the UV kernels in the other domain reflect the successive energization of the still disorganized footpoints. During the last C flare (interval D), the situation is different again. Now, both the northern and the southern UV kernels show a systematic motion parallel to each other and create flare ribbons. Therefore, we speculate that in addition to the still high shear of the magnetic arcade in this flare, consecutively reconnected field lines are now rooted side by side in both polarity domains (see Figure 9(c)). This "simpler" or "disentangled" configuration of the magnetic arcade may be a direct consequence of the magnetic reconnection processes in the three previous events. If so, this series of homologous flares demonstrates the evolution of a both highly sheared and heavily entangled magnetic arcade to a still sheared but more organized arcade.

An open question remains. The UV kernel motion in the positive polarity reversed direction in each subsequent event. This observation indicates that the reconnection was triggered at alternating sides of the arcade, but it is unclear whether this alternation occurred systematically or accidentally.

6. CONCLUSION

We interpret the observed chromospheric re-brightenings as a series of four homologous C flares, occurring within 2.5 hr due to the repeated triggering of magnetic reconnection in a loop arcade, which is characterized by a complicated magnetic configuration. We suggest that continuous shearing of the arcade, induced by horizontal, photospheric flows in the vicinity of the nearby sunspot, rebuilds the "preflare" conditions after each member of the series. In addition to the high shear, the loops of the arcade appear to be heavily entangled in the first event, but the motion pattern of the UV kernels indicates that the reconnection process in each flare increases the regularity of the loops in the arcade. Therefore, we conclude that this series of homologous flares demonstrates the evolution of a both highly sheared and heavily entangled magnetic arcade to a still sheared but more organized arcade.

We thank the anonymous referee for very constructive comments that helped to improve the manuscript. C.H.M. thanks the *TRACE* and *SOHO* missions for their open data policy. C.H.M. also thanks the Global High Resolution Hα Network, operated by the Big Bear Solar Observatory, New Jersey Institute of Technology, for providing BBSO Hα images. C.H.M. and A.M.V. gratefully acknowledge the Austrian *Fonds zur Förderung der wissenschaftlichen Forschung* (FWF grant P20145-N16) for supporting this project. M.B. acknowledges support from the European Commission through the SOLAIRE Network (MTRN-CT-2006-035484) and from the grant no. 205/07/1100 by the Grant Agency of the Czech Republic. The research leading to these results has also received funding from the European Commission's Seventh Framework Programme (FP7/2007-2013) under the grant agreement no. 218816 (SOTERIA project, www.soteria-space.eu).

REFERENCES

Bárta, M., Vršnak, B., & Karlický, M. 2008, A&A, 477, 649
Benz, A. O. 2000, in Encyclopedia of Astronomy and Astrophysics, Vol. 3, ed. Paul Murdin (Bristol: Institute of Physics Publishing), 2529
Berger, T. E., & Lites, B. W. 2003, Sol. Phys., 213, 213
Bogachev, S. A., Somov, B. V., Kosugi, T., & Sakao, T. 2005, ApJ, 630, 561
Carmichael, H. 1964, in Proc. AAS-NASA Symp. 50, The Physics of Solar Flares, ed. W. N. Hess (Washington, DC: National Aeronautics and Space Administration, Science and Technical Information Division), 451
Choe, G. S., & Cheng, C. Z. 2000, ApJ, 541, 449
Denker, C., Johannesson, A., Marquette, W., Goode, P. R., Wang, H., & Zirin, H. 1999, Sol. Phys., 184, 87
Dennis, B. R., Veronig, A., Schwartz, R. A., Sui, L., Tolbert, A. K., Zarro, D. M., & Rhessi Team 2003, Adv. Space Res., 32, 2459
Fletcher, L., & Hudson, H. S. 2002, Sol. Phys., 210, 307
Forbes, T. G., & Lin, J. 2000, J. Atmos. Sol.-Terr. Phys., 62, 1499
Forbes, T. G., & Priest, E. R. 1984, in Solar Terrestrial Physics: Present and Future, ed. D. M. Butler & K. N. Papadopoulos (NASA RP-1120; Washington, DC: NASA), 1
Gan, W. Q., Li, Y. P., & Miroshnichenko, L. I. 2008, Adv. Space Res., 41, 908
Grigis, P. C., & Benz, A. O. 2005, ApJ, 625, L143
Guidice, D. A., Cliver, E. W., Barron, W. R., & Kahler, S. 1981, BAAS, 13, 553
Handy, B. N., et al. 1999, Sol. Phys., 187, 229

Hirayama, T. 1974, Sol. Phys., 34, 323
Hudson, H. S. 1991, Sol. Phys., 133, 357
Jiřička, K., Karlický, M., Kepka, O., & Tlamicha, A. 1993, Sol. Phys., 147, 203
Karlický, M. 2004, A&A, 417, 325
Khan, J. I., Vilmer, N., Saint-Hilaire, P., & Benz, A. O. 2002, A&A, 388, 363
Kliem, B., Karlický, M., & Benz, A. O. 2000, A&A, 360, 715
Kopp, R. A., & Pneuman, G. W. 1976, Sol. Phys., 50, 85
Krucker, S., Hurford, G. J., & Lin, R. P. 2003, ApJ, 595, L103
Lee, J., & Gary, D. E. 2008, ApJ, 685, L87
Martres, M. J. 1989, Sol. Phys., 119, 357
Miklenic, C. H., Veronig, A. M., & Vršnak, B. 2009, A&A, 499, 893
Miklenic, C. H., Veronig, A. M., Vršnak, B., & Hanslmeier, A. 2007, A&A, 461, 697
Pohjolainen, S. 2003, Sol. Phys., 213, 319
Ranns, N. D. R., Harra, L. K., Matthews, S. A., & Culhane, J. L. 2000, A&A, 360, 1163
Saba, J. L. R., Gaeng, T., & Tarbell, T. D. 2006, ApJ, 641, 1197
Scherrer, P. H., et al. 1995, Sol. Phys., 162, 129
Sturrock, P. A. 1966, Nature, 211, 695
Temmer, M., Veronig, A. M., Vršnak, B., & Miklenic, C. 2007, ApJ, 654, 665
Waldmeier, M. 1938, Z. Astrophys., 16, 276
Wang, L. 2009, ApJ, 694, 247
Woodgate, B. E., et al. 1984, Adv. Space Res., 4, 11
Yashiro, S., Gopalswamy, N., Michalek, G., St. Cyr, O. C., Plunkett, S. P., Rich, N. B., & Howard, R. A. 2004, J. Geophys. Res. (Space Phys.), 109, 7105